Microgravity Science and Technology (2020) 32:1175–1184
https://doi.org/10.1007/s12217-020-09840-w

ORIGINAL ARTICLE

Quasi-Adiabatic External State Preparation of Ultracold Atoms in Microgravity

A. R. Pollard[1] · E. R. Moan[1] · C. A. Sackett[1] · E. R. Elliott[2] · R. J. Thompson[2]

Received: 30 July 2020 / Accepted: 30 September 2020 / Published online: 21 October 2020

Abstract

The Cold Atom Laboratory on the International Space Station produces ultracold gases of rubidium and potassium in a tight magnetic trap near the surface of a magnetic chip. In order to use these samples in long-duration field-free experiments, the atoms must be moved away from the chip, expanded to larger volume, and released from the trap. We describe how these goals can be achieved using quasi-adiabatic techniques. For rubidium atoms, we demonstrate a displacement of 0.6 mm and expansion into a trap with a mean oscillation frequency of 6.4 Hz. The center-of-mass release velocity and the condensate expansion velocity are about 0.2 mm/s each. An unexpectedly large background magnetic field gradient is observed, which limits the usable interaction time for the released atoms.

Keywords Ultracold atoms · Cold atom laboratory · Adiabatic cooling

Introduction

A microgravity environment offers significant benefits for ultracold atom experiments and applications (Müntinga et al. 2013; Becker et al. 2018; Condon et al. 2019; Aveline et al. 2020). It allows for long interaction times with atoms in a localized volume, without the need for an external field to support against gravity. This is advantageous for precision measurements which work best in zero field, and for experiments investigating Feshbach studies (D'Incao et al. 2017; Mossman et al. 2016) and 'bubble' geometry traps (Lundblad et al. 2019) where gravitational support would be impossible or add complexity. Microgravity is also an ideal environment for atom interferometry, which encompasses a broad range of applications such as inertial navigation, gravity gradient mapping, equivalence principle tests, and recoil frequency measurements (Cronin et al. 2009). Finally, it should be possible to attain extremely low temperatures in microgravity, since an atomic gas can be expanded to larger volumes than possible in terrestrial gravity (Müntinga et al. 2013; Ammann and Christensen 1997; Leanhardt et al. 2003; Sackett et al. 2018).

The Cold Atom Laboratory (CAL) is an ultracold atom apparatus installed on the International Space Station (Aveline et al. 2020; Elliott et al. 2018). It uses atom chip technology to produce Bose-Einstein condensates of ^{87}Rb (Fortagh and Zimmermann 2007), and also has the capability to produce cold gases of ^{39}K. It can be operated remotely in real time by staff at the Jet Propulsion Laboratory, who work with a group of principal investigators to develop and run experimental sequences. Resulting data are collated and forwarded to the principal investigators on a weekly time scale. CAL was launched in May 2018, produced its first condensate in July 2018, and began a campaign of principal investigator experiments in October 2018. This campaign ran until November 2019, when operations were temporarily halted to allow installation of an upgraded science module.

During the campaign, a substantial effort focused on extracting a usable sample of atoms with near-zero velocity. The apparatus produces condensates in a tight magnetic trap about 0.2 mm from the surface of the atom chip. This is too close to the surface for easy access with a laser beam, so it is necessary to move the atoms further away. Also, when the trap is turned off the condensate atoms will expand due to their repulsive interactions (Dalfovo et al.

Supported by NASA, grant number 1640951.

✉ C. A. Sackett
sackett@virginia.edu

[1] Physics Department, University of Virginia, Charlottesville, VA 22904 USA

[2] Jet Propulsion Laboratory, California Institute of Technology, Pasadena, CA 91109, USA

1999). If the atoms have a significant velocity due to either the displacement or the expansion, then the time they are accessible for subsequent experiments will be limited. This would negate one of the chief benefits of microgravity. In addition, atom interferometry works best if the velocity spread of the atomic sample is very small compared to the photon recoil velocity (Cronin et al. 2009; Hughes et al. 2007). For these reasons, it is necessary to develop techniques to displace and expand the atoms in a controlled way, so as to provide a sample of atoms in a specified location with low velocities.

There have been two complementary approaches proposed for how this sample preparation step might be achieved. One is quasi-adiabatic (QA) expansion, where the trap is displaced and relaxed over a time scale that is long compared to the oscillation period of the atoms in the trap, such that the atoms remain close to their ground state at all times (Leanhardt et al. 2003; Sackett et al. 2018). Another is the shortcut-to-adiabaticity (STA) technique, in which the trapping fields are changed quickly in a controlled way such that the magnetic forces displace, expand, and bring the atoms back to rest over the course of the motion (Müntinga et al. 2013; Ammann and Christensen 1997; Aoki et al. 2006). Both of these approaches were explored during the CAL campaign, and we report here on the quasi-adiabatic expansion results.

The two approaches are subject to different limitations. The QA approach requires the ability to greatly relax the confinement strength of the magnetic trap, which can be achieved by reducing the trap fields. However, this is infeasible once the trap field strength becomes comparable to the background magnetic field of the apparatus. The CAL apparatus features magnetic shielding, but it also has field sources inside the shield. Design estimates specified a background field below 10 mG with a gradient below 1 G/m, but our results indicate that the actual background gradient is considerably larger. In contrast, the STA technique is less sensitive to background fields since only relatively large trapping fields are used. However, the STA approach requires precise understanding and control of the trap fields themselves, while the QA approach is less sensitive to the details of the trap. While STA is typically faster, the QA approach is easier to implement with multiple species; this is relevant to equivalence principle tests that would use both Rb and K atoms simultaneously (Lämmerzahl 2003; Rudolph et al. 2011; Williams et al. 2016). It is these differences that make both approaches worth exploring.

Our results show that the QA approach is indeed constrained by the background fields, limiting the minimum obtainable atomic velocity spread to about 0.2 mm/s. This is sufficient for many proposed experiments, but not below what has been achieved on Earth. Moreover, the background gradient causes the atoms to accelerate and this further restricts the interaction time. Although CAL features two cameras which can provide three-dimensional imaging, one of the cameras was not brought into operation during the campaign, so we have limited knowledge about one direction of motion. Nonetheless we are able to determine the full three-dimensional background field by combining observations of how the trap behaves with observations of how the untrapped atoms accelerate.

The remainder of the paper is organized around the three phases of the QA expansion experiments. Section "Displacing Atoms from the Chip" discusses the displacement of the atoms away from the chip, which is carried out in a trap that is as tight as practical in order to minimize motional excitation. Section "Expansion at Fixed Position" describes the relaxation of the trap to achieve adiabatic cooling. Section "Motion After Trap Release" describes the free motion of the atoms after the trap fields are turned off. Section "Discussion" provides conclusions and an outlook for further progress.

Displacing Atoms from the Chip

The CAL magnetic trap is produced by an atom chip in conjunction with bias fields from pairs of electromagnetic coils. The chip geometry is shown in Fig. 1. It uses two current elements, a Z-shaped wire with current I_Z and a straight 'dimple' wire carrying current I_D. We model the trap fields using the Biot-Savart law. Since the distance from the atoms to the wires is large compared to the width of the wires, it is sufficient to approximate the wires as line sources. It is also sufficient to model the bias fields as uniform, which we verified by comparing to a calculation using the physical bias coil geometry. The trap model works by calculating the vector field $\mathbf{B}$ at a given position $\mathbf{r}$, numerically finding the trap center $\mathbf{r}_c$ where the potential energy $U = \mu|\mathbf{B}|$ is minimized, and then diagonalizing the Hessian matrix $\partial^2 U/\partial r_i \partial r_j$ to find the trap oscillation

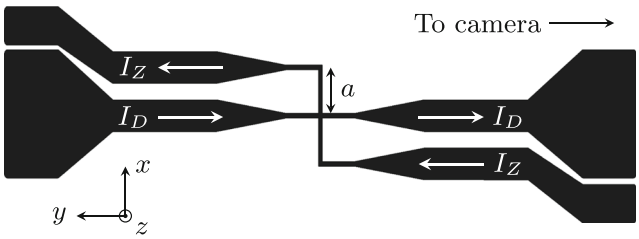

Fig. 1 Atom chip used on CAL. Currents I_Z and I_D flow through the indicated traces. The axes define the coordinate system used here. The origin of the coordinate system is at the point where the wires cross. The trapped atoms are located at $z > 0$, above the plane of the page. The location of the imaging camera is indicated and the length a is 1.1 mm

frequencies and principal directions. Here μ is the magnetic moment of the trapped spin state, which is close to the Bohr magneton for ^{87}Rb atoms in the $F = 2, m_F = 2$ state as used here.

For most of our work, Bose-Einstein condensates are produced in a trap with $I_Z = 3.2$ A, $I_D = 0.4$ A, and bias fields $B_x = 8.6$ G, $B_y = 28.8$ G, $B_z = 1.44$ G. We did not characterize this trap experimentally, but the model gives oscillation frequencies $(\omega_x, \omega_y, \omega_z) = 2\pi \times (160, 780, 800)$ Hz. The trap center is 0.2 mm from the chip surface. Evaporative cooling typically produces a cloud of about 4×10^4 trapped Rb atoms with a condensate fraction of about 25%. However, the number and condensate fraction sometimes fluctuated substantially from run to run. The work described here did not require a condensate except in the weakest traps studied, for which only the condensate provided sufficient atom density for detection.

In the first phase of the QA expansion, we displace the atoms away from the chip. The distance scale over which the trapping fields change character is set by the wire spacing $a = 1.1$ mm, and the maximum possible displacement is about $2a$. We target a final trap location at $z = 0.8$ mm, which is large enough to accommodate a laser beam but remains in the region where the trap fields remain relatively simple. In this region, the trap center z_c depends on the chip currents and bias fields approximately as $z_c \propto I/B$, so typically we move the atoms away from the chip by uniformly reducing the bias fields. The imaging camera views the xz plane, so motion of the atoms along y is undetected.

We design the displacement to minimize the excitation of center-of-mass "sloshing" motion of atoms in the trap. Figure 2 shows typical data used to measure the excitation amplitude. Here the atoms are displaced and then held in a static trap for a variable time t. The trap is turned off and the atoms allowed to evolve freely for a fixed time of flight τ. The atoms are probed using absorption imaging, and the results fit to a Gaussian or Thomas-Fermi wavefunction to find the center of the distribution. The observed centers are typically reproducible with about 5 μm variations in repeated measurements. The centers are fit to a sinusoid function to determine the oscillation frequency ω and amplitude A_τ. The amplitudes are corrected for the time of flight to find the oscillation amplitude in the trap,

$$A = \frac{A_\tau}{\sqrt{1+\omega^2\tau^2}}. \tag{1}$$

Typically we use $\tau = 16$ ms.

We implemented a simple dynamical model for the displacement process which treats the center of mass of the cloud as a classical particle. We approximate the three-dimensional trap potential as harmonic, with confinement frequencies and center position which vary in time according to our field model. We then solve Newton's equations of motion for the trajectory of the particle. This model neglects any internal dynamics of the atom cloud. It is possible for parametric amplification and/or trap anharmonicity to induce internal excitations, but we did not observe such effects. A non-linear Schrödinger equation model for the condensate confirmed that none should be expected under our conditions. (Delikatny and Forbes 2020)

In previous work (Sackett et al. 2018), we developed a quasi-adiabatic trajectory that was calculated to generate approximately one quantum $\hbar\omega$ of excitation energy over the entire expansion. That work assumed that it would be possible to adiabatically switch the chip current from the initial Z wire to another trace with a larger size a, but the implementation of the current drivers in CAL did not permit such a switch. In addition, our previous analysis assumed arbitrarily smooth behavior of the chip currents and bias fields as a function of time. As implemented, the CAL system requires parameters to be varied using a limited number of linear ramps. We had approximately forty such ramp steps available for the work here. To satisfy this constraint, it was necessary to modify the smooth ramps previously developed in a way that minimized additional excitation. We explored various methods for doing so. Figure 3a-b shows how the calculated trap center and oscillation frequency vary during a sequence of $M = 8$ ramp stages. For these measurements, the initial trap had $I_Z = 3.2$ A, $I_D = 0.4$ A, and $\mathbf{B} = (10.75, 36, 1.8)$ G. The dashed curves are determined from the underlying smooth function, here given by

$$\begin{aligned} I_j(t) &= I_j(0)(1-0.5u) \\ B_j(t) &= B_j(0)(1-0.9u), \end{aligned} \tag{2}$$

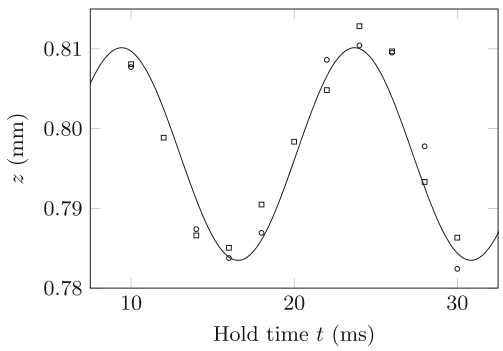

Fig. 2 Example data for a trap oscillation measurement in the displaced trap. The circle and square points are measured values obtained during two different runs. The curve is a sinusoidal fit yielding a frequency of 70.0 Hz and an amplitude of 13(4) μm. This corresponds to an in-trap amplitude of 1.9(7) μm

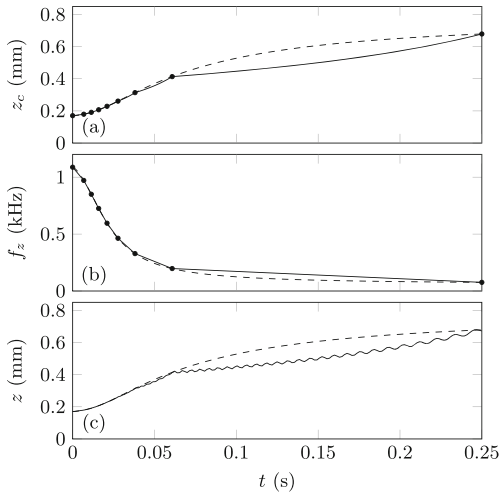

Fig. 3 Displacement ramp model. Parts (**a**) and (**b**) show the calculated trap position z_c and oscillation frequency $f_z = \omega_z/2\pi$ as function of time. The dashed curves are the smooth functions calculated using Eq. 3, while the solid curves come from a linearization with $M = 8$ stages. The dots indicate transitions between stages. Part (**c**) shows the calculated trajectory of the atoms in the moving trap, again for the smooth and $M = 8$ cases

where j labels the different current and field components and u is a scaling function (Sackett et al. 2018)

$$u(t) = \frac{1}{\theta}\tan^{-1}\left[\left(\frac{t}{T_1}\right)^{1/\gamma}\tan\theta\right] \tag{3}$$

with parameters $\theta = \pi/2 - 0.03$, $\gamma = 0.7$, and $T_1 = 0.25$ s. Here T_1 is the total duration of the displacement sequence. In this case the ramp stages consisted of equal steps in u. Part (c) of the figure shows the resulting model trajectory $z(t)$. It can be seen that the linearized trajectory results substantially larger oscillations than the smooth trajectory.

Figure 4 shows experimental results obtained when the number of linear stages M was varied. The classical model predicts that the final amplitude is somewhat sensitive to the details of the trap and the exact durations of the linear stages, reflecting the fact that the motion is only quasi-adiabatic. To accommodate this, we slightly varied the ramp parameters in the model and obtained a range of values indicated by the vertical bars in the plot. In general, the best and most reliable performance is obtained with the largest number of stages. For comparison, the calculated final in-trap amplitude for a smoothly-varying ramp ranges from 0.8 to 1.2 μm.

We explored various different ramp shapes and linearization schemes. While the ramp shape was not observed to be very important, the linearization method had some impact. For a physically motivated scheme, we consider a trap whose center is moving at constant velocity v_1 and then suddenly changes to v_2. In the frame of the trap, the average change in the energy of an atom with mass m will be $\Delta E = (1/2)m(v_2 - v_1)^2$. We therefore linearized the trap displacement trajectory so as to minimize $\sum_{i=1}^{M-1}(v_{i+1} - v_i)^2$, where v_i is the speed at which the trap center moves during ramp stage i. We found it best to keep the chip currents at their maximum values during the displacement phase, since that provided the largest confinement frequency at a given trap position z_c. We also explored different displacement times T_1, and found that the final oscillation amplitude consistently increased for ramp times shorter than 0.25 s, while using longer times up to 0.5 s did not consistently lead to improvements.

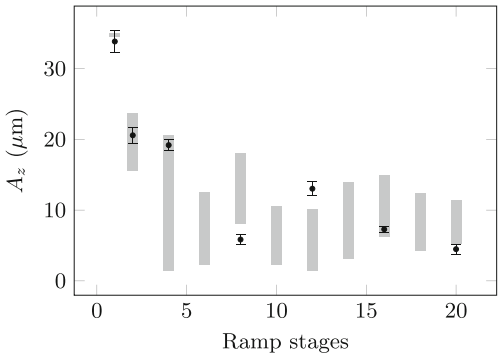

Fig. 4 Oscillation amplitude of the atoms as a function of the number of linear ramp stages, for ramps as in Fig. 3. On the vertical axis, A_z is the oscillation amplitude along the z axis for atoms in the trap. Points are measured values inferred from data such as Fig. 2 after time-of-flight adjustment. The vertical bands show the ranges of values obtained in the numerical model as the trajectory parameters are slightly varied

The first twenty stages of Table 1 show the displacement sequence for which we obtained the best performance. The corresponding trap behavior is illustrated in Fig. 5. Here the chip currents are held constant while the fields vary as $B_i = B_i(0)(1 - 0.8u)$, for u as in Eq. 3 but with $\theta = \pi/2 - 0.05$ and $\gamma = 0.6$. The initial field values are given in the table. This sequence results in a motional amplitude of 1.9 μm in a 70 Hz trap, as seen in Fig. 2. The corresponding center-of-mass energy is 3.5 nK $\approx \hbar\omega_z$, and the velocity amplitude is 0.8 mm/s. A condensate in this trap has a Thomas-Fermi chemical potential of about 16 nK, which gives an expansion velocity of 0.9 mm/s after sudden release (Dalfovo et al. 1999). These velocities are large enough to restrict free-fall interaction times to a few tenths of a second and to impact atom interferometry performance. To obtain yet lower velocities, we further expanded the trap.

Expansion at Fixed Position

We implemented a second stage of adiabatic expansion, with the atoms nominally held in place at $z = 0.8$ mm. This can be achieved by uniformly reducing all the chip

Table 1 Parameters used for complete expansion. A ramp step ends at time T, and I_Z, I_D, B_x, B_y and B_z are the current and field parameters at the end of the step. Our field model is used to calculate the trap position z_c, where x_c and y_c are not shown since they are predicted to remain close to zero. The calculated oscillation frequencies are listed as f_x, f_y and f_z, although at the end of the expansion the principal axes of the trap are no longer perfectly aligned to the coordinate axes

t (s)	I_Z (A)	I_D (A)	B_x (G)	B_y (G)	B_z (G)	z_c (mm)	f_x (Hz)	f_y (Hz)	f_z (Hz)
0.000	3.20	0.400	8.60	28.80	1.44	0.211	162.4	775.4	799.6
0.003	3.20	0.400	8.53	28.57	1.43	0.213	160.6	765.9	790.0
0.008	3.20	0.400	8.32	27.87	1.39	0.218	155.1	737.9	761.4
0.015	3.20	0.400	7.77	26.01	1.30	0.233	140.7	664.9	687.1
0.021	3.20	0.400	7.14	23.91	1.20	0.251	125.4	585.9	606.5
0.027	3.20	0.400	6.58	22.05	1.10	0.271	112.3	518.6	537.9
0.034	3.20	0.400	5.75	19.26	0.963	0.306	93.9	423.1	440.3
0.056	3.20	0.400	3.94	13.21	0.660	0.424	59.4	242.0	254.2
0.067	3.20	0.400	3.39	11.35	0.567	0.480	50.3	194.5	204.5
0.075	3.20	0.400	3.11	10.41	0.521	0.514	45.9	172.2	181.0
0.085	3.20	0.400	2.83	9.48	0.474	0.553	41.7	151.1	158.5
0.098	3.20	0.400	2.55	8.55	0.428	0.598	37.7	131.1	137.0
0.107	3.20	0.400	2.41	8.09	0.404	0.623	35.7	121.5	126.5
0.118	3.20	0.400	2.28	7.62	0.381	0.651	33.7	112.2	116.3
0.133	3.20	0.400	2.14	7.16	0.358	0.682	31.7	103.2	106.4
0.143	3.20	0.400	2.07	6.92	0.346	0.698	30.7	98.7	101.4
0.154	3.20	0.400	2.00	6.69	0.335	0.716	29.7	94.4	96.6
0.169	3.20	0.400	1.93	6.46	0.323	0.734	28.7	90.1	91.7
0.187	3.20	0.400	1.86	6.22	0.311	0.754	27.7	85.8	86.9
0.213	3.20	0.400	1.79	5.99	0.300	0.774	26.7	81.7	82.2
0.250	3.20	0.400	1.72	5.76	0.288	0.796	25.7	77.5	77.5
0.258	3.056	0.382	1.64	5.50	0.275	0.796	25.1	75.7	75.8
0.274	2.481	0.310	1.34	4.47	0.223	0.796	22.6	68.2	68.2
0.299	1.619	0.202	0.885	2.91	0.145	0.796	18.3	54.9	54.9
0.323	1.043	0.130	0.581	1.88	0.0936	0.796	14.7	44.0	44.0
0.341	0.756	0.0940	0.429	1.36	0.0677	0.795	12.5	37.3	37.3
0.355	0.612	0.0760	0.353	1.10	0.0548	0.794	11.2	33.4	33.4
0.372	0.468	0.0580	0.277	0.842	0.0418	0.794	9.8	29.0	29.0
0.399	0.325	0.0400	0.201	0.583	0.0288	0.792	8.1	23.9	23.9
0.416	0.264	0.0324	0.169	0.474	0.0234	0.790	7.3	21.5	21.5
0.440	0.203	0.0248	0.137	0.365	0.0179	0.792	6.4	18.5	18.5
0.457	0.173	0.0210	0.121	0.310	0.0152	0.789	5.9	16.9	16.9
0.479	0.142	0.0172	0.105	0.256	0.0124	0.786	5.3	15.2	15.2
0.509	0.112	0.0134	0.0888	0.201	0.0097	0.781	4.7	13.3	13.3
0.530	0.0970	0.0115	0.0808	0.174	0.0083	0.784	4.3	12.1	12.1
0.557	0.0818	0.00960	0.0728	0.146	0.0070	0.775	4.0	11.1	11.1
0.594	0.0666	0.00770	0.0647	0.119	0.0056	0.776	3.6	9.7	9.7
0.649	0.0514	0.00580	0.0567	0.0917	0.0042	0.780	3.0	8.0	8.1
0.740	0.0363	0.00390	0.0487	0.0644	0.0029	0.755	2.6	6.7	6.7
0.943	0.0211	0.00200	0.0407	0.0370	0.0015	0.752	1.7	4.4	4.5

currents and bias fields together, but as discussed in Sackett et al. (2018), it is advantageous to leave the B_x bias field relatively large to minimize the perturbing effect of background fields. A quasi-adiabatic trajectory for this expansion step was developed in Sackett et al. (2018), but again it required modification into a sequence of linear

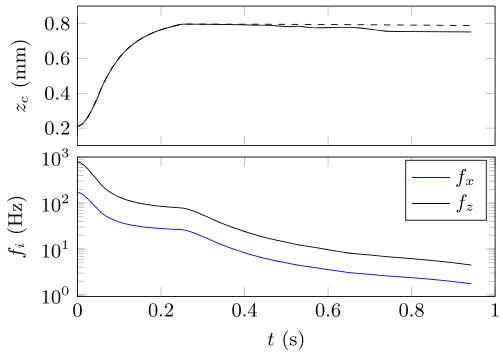

Fig. 5 Calculated trap location z_c and oscillation frequencies f_x, f_y, and f_z for the complete expansion ramp of Table 1. At the end of the expansion, the principle axes of the trap are rotated by about 30° in the xy plane, so the f_i labels are not entirely accurate. In the upper plot, the irregular behavior of z_c at later times is due to rounding of the programmed current driver values. The ideal behavior is shown as the dashed curve. This problem could have been avoided, but any impact on the experimental performance was small compared to the effect of background fields, see Fig. 7

ramps. We used twenty ramps for this part of the expansion, as shown in the second half of Table 1 and Fig. 5. The underlying smooth functions are here

$$\begin{aligned} I_Z(u) &= I_Z(0)(1-0.9984u) \\ I_D(u) &= I_D(0)(1-u) \\ B_x(u) &= B_x(0)(1-0.9813u) \\ B_y(u) &= B_y(0)(1-0.9986u) \\ B_z(u) &= B_z(0)(1-0.9998u). \end{aligned} \tag{4}$$

The $u = 0$ values for each parameter are the values at the end of the first ramp. We found good performance in the model with a time scaling

$$t = T_1 + 0.2277\, T_2 \left[\tan\left(\frac{\theta u}{10-9u}\right)\right]^{\gamma}, \tag{5}$$

with $\theta = \pi/2 - 0.01$ and $\gamma = 0.6$. The rational function in the tangent acts to further slow down the expansion as u approaches 1. In this expansion u runs from 0 to 0.995; the parameters at $u = 1$ correspond to a very weak trap that was not successfully observed. The duration of the expansion sequence (with $u_{\max} = 0.995$) is T_2, while T_1 is the duration of the displacement sequence described previously.

The expansion duration is constrained by the lifetime of atoms in the trap. We measured the lifetime by holding the atoms in a weak trap where three-body losses were negligible. We observed an exponential decay time of about 4 s, which is consistent with the estimated vacuum pressure of about 10^{-7} Pa. In order to leave time for further experiments, we aimed to complete the entire state preparation in about 1 s.

Table 1 shows the parameters for the forty steps used in the final expansion, along with the predicted trap centers and frequencies. For comparison, Table 2 shows the experimentally measured positions, frequencies, and oscillation amplitudes at selected stages. Trap A is the configuration reached at the end of "Displacing Atoms from the Chip" above, and trap E is the final trap configuration. While the measurements generally agree with the model in the more confining traps, we observed the trap position to move towards the chip as the f_z frequency dropped below 20 Hz. Because of this motion, the chip gradient increased and the trap confinement is greater than predicted. The motion of the trap accelerated as the fields were made weaker, which prevented us from reliably seeing atoms in traps weaker than those shown. We attribute this effect to a background magnetic field that was larger than expected, as discussed further in "Motion After Trap Release" below.

We did reliably observe expansion into trap E, with measured frequencies $f_x = 2.7$ Hz and $f_z = 9.9$ Hz. The background field model developed below indicates that $f_y \approx 7.5$ Hz here, which implies a chemical potential $\mu = 1.2$ nK for 10^4 condensate atoms. From this we calculate rms condensate expansion velocities $(v_x, v_y, v_z) = (0.08, 0.15, 0.18)$ mm/s. However, from trap oscillation measurements as in Fig. 2, we find that the oscillation amplitudes in trap E correspond to velocities $v_x = 0.26$ mm/s and $v_z = 0.75$ mm/s (Dalfovo et al. 1999). This excitation is due to the anomalous displacement of the trap center from the background field. Fortunately, the phase of the oscillation is stable, so it is possible to time the trap release to minimize the center-of-mass velocity. Over

Table 2 Experimental trap characterization. Parameters are as in Table 1, but here the trap positions and frequencies are measured values. The oscillations amplitudes A_i are calculated as in Eq. 1

Label	I_Z (mA)	I_D (mA)	B_x (mG)	B_y (mG)	B_z (mG)	x_c (mm)	z_c (mm)	f_x (Hz)	f_z (Hz)	A_x (μm)	A_z (μm)
A	3200	400	1710	5720	286	0.002	0.797	25.8	70.0	0.9	1.9
B	320	40.0	172	576	29	0.013	0.815	-	31.1	-	7.5
C	128	16.0	64.5	216	11	0.005	0.758	3.5	21.4	12	7.2
D	36.3	3.9	49	64	2.9	-0.062	0.592	3.6	15.7	27	6.9
E	21.1	2.0	41	37	1.5	-0.148	0.479	2.7	9.9	16	12

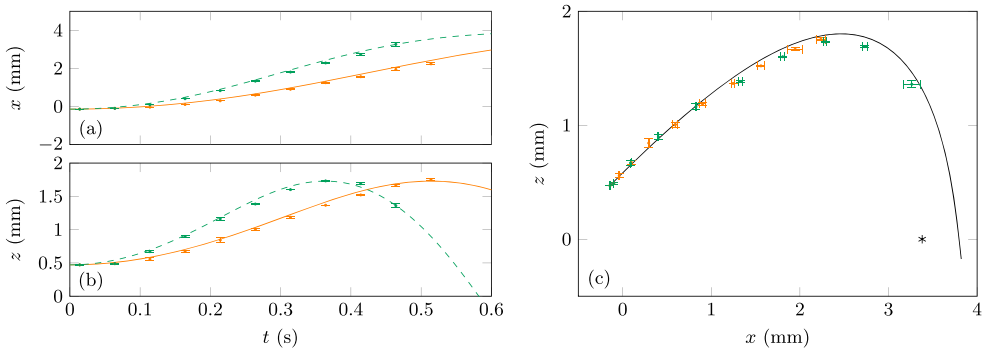

Fig. 6 Time of flight motion of the atoms after the trapping fields are reduced to zero at time $t = 0$. Plots (a) and (b) show x and z as functions of time. Orange points are atoms in the $m = 1$ spin state and green points are atoms in the $m = 2$ state. Error bars are estimated from the variance of repeated measurements. Curves are model trajectories assuming the presence of a background gradient as in Eq. 6. Plot (c) shows the trajectory $z(x)$, illustrating that the $m = 1$ and $m = 2$ atoms follow the same path. The star symbol shows the location of the field zero $\mathbf{r}_0$ in the xz plane

the course of a month, the phase of the oscillation along z fluctuated by about 0.2 rad, which corresponds to a release velocity fluctuation $\sigma_{v_z} = 0.15$ mm/s.

Velocity components of 0.2 mm/s are about 3% of the recoil velocity for 780 nm light, which is low enough to have minimal impact on atom interferometer performance. If the atoms were to interact with a laser beam having a waist of 1 mm, then over a 1 s interrogation time the atomic motion would lead to a relative intensity variation below 10%. Alternatively, in about 2 s portions of the atom cloud could impact the atom chip. On this basis, we argue that the quasi-adiabatic scheme demonstrated here can be used for experiments of up to roughly 1 s duration. However, particular applications may have more demanding requirements. For instance, equivalence principle tests require two species with relative velocity of 1 μm/s or less (Williams et al. 2016; Loriani et al. 2020). More sophisticated techniques will likely be required for such experiments.

Motion After Trap Release

In order to test the state preparation technique, we turned off the trap and observed the subsequent motion of the atoms. Two non-ideal features occurred. First, the rapid switchoff of the trap fields induced non-adiabatic spin flip transitions in the atoms, causing multiple spin states to be populated. Roughly equal populations were left in the $m = 1$ and $m = 2$ states, with a small population sometimes observable in $m = 0$. Second, an unexpectedly large background gradient field caused the atoms to accelerate. The acceleration could be unambiguously attributed to a field gradient because it was closely proportional to the atoms' magnetic moment. This led to spatial separation of the spin components as in the Stern-Gerlach effect.

Figure 6 shows the trajectories of the released atoms. Their acceleration is not constant, indicating that the field magnitude has nontrivial spatial variations. We model the background field as

$$\mathbf{B}(\mathbf{r}) = G(\mathbf{r} - \mathbf{r}_0) = \begin{bmatrix} G_{xx} & G_{xy} & G_{xz} \\ G_{xy} & G_{yy} & G_{yz} \\ G_{xz} & G_{yz} & G_{zz} \end{bmatrix} \begin{bmatrix} x - x_0 \\ y - y_0 \\ z - z_0 \end{bmatrix}, \quad (6)$$

where G is a symmetric matrix. Maxwell's equations require $\mathrm{Tr}\, G = 0$. The vector $\mathbf{r}_0$ gives the location where the background field is zero. For atoms with $m > 0$, the field forms a non-harmonic trap centered at $\mathbf{r}_0$.

Because we lack information about the y component of the motion, the time-of-flight trajectory is insufficient to determine all of the gradient parameters. However, the background field will also affect the location and confinement strength of the trap, and this does depend on the y component of the field. We performed a combined fit to the time-of-flight trajectory, the trap center (x_c, z_c) and the trap frequencies (f_x, f_z). For this fit we used the trap E configuration, since it is most sensitive to the background field. The best fit results are shown in

Table 3 Parameters of the background gradient field from Eq. 6, as determined using time-of-flight and trap performance measurements. Values in parentheses are the fit uncertainties

x_0 (mm)	y_0 (mm)	z_0 (mm)	G_{xx} (G/m)	G_{yy} (G/m)	G_{xy} (G/m)	G_{xz} (G/m)	G_{yz} (G/m)
3.3(4)	2.9(7)	0.00(1)	0.4(1.2)	−7.6(6)	−0.1(1)	10(1)	−2(1)

Table 3. The fitted trajectories are shown as curves in Fig. 6, and agree well with the measurements. Figure 7 shows the calculated impact of the background field on the expansion ramp, along with measured parameters for traps A, B, D and E. Agreement is reasonably good, particularly given that only the trap E results were part of the fit. Errors in the fit parameters were estimated via a Monte Carlo technique, where the measured data values were randomly varied according to their uncertainty and then refit.

Using the fitted field parameters, we calculate the initial acceleration to be $\mathbf{a} = (46, 24, 35)$ mm/s^2 for $m = 2$ atoms. While the net acceleration is only about $6 \times 10^{-3} g$, this is substantially larger than the expected residual gravity at CAL of order $10^{-6} g$ (McPherson et al. 2015). The resulting velocity exceeds the expected release velocity after about 4 ms, and severely limits the usable interaction time of a subsequent measurement. We discuss potential mitigation strategies below.

The source of this background field is not clear. The dominant contribution to the field was expected to be from an ion pump magnet located about 20 cm away, which in isolation produced a gradient of about 1 G/m at the trap location. In comparison, the peak gradient of the modeled field is 14 G/m. It was not possible to measure the background field in the fully assembled CAL unit prior to launch.

It is noteworthy that we are able to characterize the mG-level background field using only trap characterization and time-of-flight analysis. In terrestrial gravity, atoms would fall out of a trap with $f_z \leq 20$ Hz, so the impact of the background field on the trap would be difficult to observe. And since the atoms would fall about 1 m during the 0.5 s time of flight, it would be impossible to use them as a probe of the local field with this method. This type of analysis can thus be viewed as particularly well-suited for the microgravity environment.

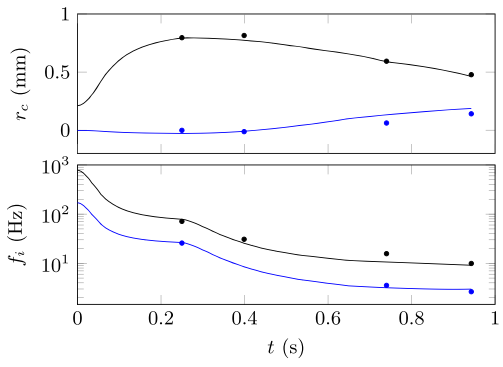

Fig. 7 Calculated trap location (x_c, z_c) and oscillation frequencies (f_x, f_y, f_z) for the expansion ramp, in the presence of the background gradient of Table 3. Blue curves are x_c and f_x, while black curves are z_c and f_z. Points are measured values corresponding to traps A, B, D and E

Discussion

In order for CAL to perform as designed, it will be necessary to reduce the impact of the anomalous background field. The apparatus has one additional pair of coils along the x axis that can be configured to provide a compensating gradient, and the chip itself can generate gradient fields using the Z and D wires. These provide three degrees of freedom that can produce a gradient G_{comp} at the trap location of the form

$$G_{\text{comp}} = \begin{bmatrix} \alpha + \beta & 0 & -0.2\gamma \\ 0 & -\alpha/2 & \gamma \\ -0.2\gamma & \gamma & -\alpha/2 - \beta \end{bmatrix}, \tag{7}$$

where α parametrizes the gradient from the coils, β the D wire, and γ the Z wire. The total gradient is minimized for $\alpha = -15$ G/m, $\beta = 15$ G/m and $\gamma = 4$ G/m, leaving a residual

$$G + G_{\text{comp}} \approx \begin{bmatrix} 0 & 0 & 9 \\ 0 & 0 & 2 \\ 9 & 2 & 0 \end{bmatrix} \text{ G/m} \tag{8}$$

which is still unacceptably large. We did not have the opportunity to explore this type of compensation on CAL.

A different approach is to transfer the atoms to the $m = 0$ state, where they experience only a quadratic Zeeman effect so the magnetic force is substantially reduced. We have used the adiabatic rapid passage (ARP) technique to transfer trapped atoms into the $m = 0$ state with an efficiency of about 50% (Aveline et al. 2020). After the trapping fields are turned off, the acceleration from the quadratic Zeeman effect is calculated to be 10^{-3} mm/s^2 for ^{87}Rb, an order of magnitude below the residual gravitational acceleration. We expect that atoms extracted via ARP from a trap such as configuration E would meet the basic requirements for further experiments such as atom interferometry. However, even the small quadratic Zeeman shift could be significant for a long-time interferometry measurement, so it will be important for the design of such experiments to take the background field into account.

The ARP experiments that were performed used atoms released from a relatively tight trap which had been non-adiabatically displaced from the chip. As a result the center-of-mass velocity was 3.1 mm/s, which is larger than desired. The velocity was also very sensitive to the trap parameters and timing. Nonetheless, $m = 0$ atoms were observed in time of flight for up to 1.2 s with no measurable acceleration. This supports the conclusion that atoms transferred to $m = 0$ from a quasi-adiabatically

expanded trap would be a suitable source for long-duration experiments. Unfortunately, we were unable to test the ARP transfer with the QA approach during this measurement campaign.

It is interesting to consider the temperature attained and the prospects for cooling further. A gas of 4×10^4 atoms in a trap with mean frequency 6.4 Hz has a condensation temperature of 10 nK. A condensate fraction of 25% then corresponds to a temperature of 9 nK, which can be compared to the temperature of 0.5 nK achieved for ^{23}Na atoms in a terrestrial experiment (Leanhardt et al. 2003). Reaching sub-nK temperatures in CAL via quasi-adiabatic expansion would require a mean trap frequency of 0.5 Hz. It does not seem possible to achieve this without additional means to compensate the background field.

In practice, however, the non-condensed fraction of the gas is too diffuse to be easily detected in such a weak trap. Furthermore, after the trap is turned off the non-condensed atoms will quickly leave the interaction region. Although the remaining condensate atoms are not in thermal equilibrium, their predicted expansion velocities correspond to a substantially lower temperature. This effective temperature is the relevant quantity for practical measurements which interact primarily with the condensate fraction. A condensate released from our trap E would have free-expansion energies of 80 pK, 150 pK and 180 pK in the x, y and z directions respectively. In comparison, the expansion velocities observed after ARP transfer from the non-adiabatically expanded trap corresponded to 230 pK along x and 720 pK along z (Aveline et al. 2020).

In addition to expanding, a released atom sample will exhibit fluctuations in the center-of-mass velocity. These fluctuations have a practical impact similar to a non-zero temperature, since they lead to uncertainty in the velocity and position of the atoms. Our estimated release velocity stabilities discussed above correspond to a temperature of about 250 pK. In the ARP experiments, the center-of-mass velocity fluctuation was measured to be $\sigma_{v_z} \approx 0.36$ mm/s, corresponding to 1.4 nK. For whatever state preparation method is used, it will be important to characterize these types of fluctuations over both short and long time scales.

As the studies described here were being performed, a parallel effort was made to implement state preparation using the STA technique. As in our work, it was not possible to implement tests with $m = 0$ atoms so time-of-flight measurement were limited by the background gradient. However, the STA technique is less sensitive to the background fields, and the results obtained suggest the possibility to reach expansion and center-of-mass energies about ten times lower than those reported here (Corgier et al. 2018; Gaaloul and Bigelow 2020). This makes the STA technique promising for obtaining the longest possible interaction times, at least for single-species experiments.

For future work, the CAL apparatus has been upgraded with a new science module that provides the capability for atom interferometry experiments. A Bragg laser beam passes through a window in the atom chip and travels at a small angle to the z axis. The beam is retro-reflected by an in-vacuum mirror. The atom chip itself has a new design, with two Z wires passing on opposite sides of the window. A condensate will be produced at one of the Z wires, and it must then be displaced both away from the chip and transversely into the center of the window. The QA methods demonstrated here can be readily modified to suit this new geometry, potentially allowing interferometry studies to proceed in parallel with the more detailed trap characterization required for the STA method. In this way we hope to maximize the utility of the system for inertial sensing and equivalence principle tests.

Acknowledgements We are grateful to the support team at Jet Propulsion Laboratory, including David Aveline, Jason Williams, Jim Kohel and Jim Kellogg. We thank Ted Delikatny and Michael Forbes at Washington State University for implementing and sharing the NLSE tests checking for internal condensate excitations. We thank Nick Bigelow and Naceur Gaaloul for sharing and discussing their STA results. We are also happy to acknowledge useful discussions with other members of the CAL PI team, especially Nathan Lundblad, Peter Engels, and Maren Mossman. Finally, we thank Mark Edwards for pointing out an error in one of the figures.

Compliance with Ethical Standards

Conflict of interests The authors declare that they have no conflict of interest.

References

Ammann, H., Christensen, N.: Delta kick cooling A new method for cooling atoms. Phys. Rev. Lett. **78**, 2088 (1997)

Aoki, T., Kato, T., Tanami, Y., Nakamatsu, H.: δ-kick cooling using the Ioffe-Pritchard potential. Phys. Rev A **73**, 063603 (2006)

Aveline, D.C., Williams, J.R., Elliott, E.R., Dutenhoffer, C., Kellogg, J.R., Kohel, J.M., Lay, N.E., Oudrhiri, K., Shotwell, R.F., Yu, N., Thompson, R.J.: Observation of Bose–Einstein condensates in an Earth-orbiting research lab. Nature **582**, 193 (2020)

Becker, D., Lachmann, M.D., Seidel, S.T., Ahlers, H., Dinkelaker, A.N., Grosse, J., Hellmig, O., Müntinga, H., Schkolnik, V., Wendrich, T., Wenzlawski, A., Weps, B., Corgier, R., Franz, T., Gaaloul, N., Herr, W., Lüdtke, D., Popp, M., Amri, S., Duncker, H., Erbe, M., Kohfeldt, A., Kubelka-Lange, A., Braxmaier, C., Charron, E., Ertmer, W., Krutzik, M., Lämmerzahl, C., Peters, A., Schleich, W.P., Sengstock, K., Walser, R., Wicht, A., Windpassinger, P., Rasel, E.M.: Space-borne Bose–Einstein condensation for precision interferometry. Nature **562**(7727), 391–395 (2018)

Condon, G., Rabault, M., Barrett, B., Chichet, L., Arguel, R., Eneriz-Imaz, H., Naik, D., Bertoldi, A., Battelier, B., Bouyer, P., Landragin, A.: All-optical Bose–Einstein Condensates in microgravity. Phys. Rev. Lett. **123**, 240402 (2019)

Corgier, R., Amri, S., Herr, W., Ahlers, H., Rudolph, J., Guéry-Odelin, D., Rasel, E.M., Charron, E., Gaaloul, N.: Fast manipulation

of Bose–Einstein condensates with an atom chip. J. Phys. **20**(5):055002 (2018)
Cronin, A.D., Schmiedmayer, J., Pritchard, D.E.: Optics and interferometry with atoms and molecules. Rev. Mod. Phys. **81**, 1051 (2009)
D'Incao, J.P., Krutzik, M., Elliott, E., Williams, J.R.: Enhanced association and dissociation of heteronuclear feshbach molecules in a microgravity environment. Phys. Rev. A **95**, 012701 (2017)
Dalfovo, F., Giorgini, S., Pitaevskii, L., Stringari, S.: Theory of Bose–Einstein, condensation in trapped gases. Rev. Mod. Phys. **71**, 463 (1999)
Delikatny, T., Forbes, M.: Private communication (2020)
Elliott, E.R., Krutzik, M.C., Williams, J.R., Thompson, R.J., Aveline, D.C.: NASA's Cold Atom Lab (CAL): system development and ground test status. npj Micrograv. **4**(1), 16 (2018)
Fortagh, J., Zimmermann, C.: Magnetic microtraps for ultracold atoms. Rev. Mod Phys. **79**, 235 (2007)
Gaaloul, N., Bigelow, N.: Private communication (2020)
Hughes, K.J., Deissler, B., Burke, J.H.T., Sackett, C.A.: High-fidelity manipulation of a Bose–Einstein, condensate using an optical standing wave. Phys. Rev. A **76**, 035601 (2007)
Lämmerzahl, C.: The Einstein equivalence principle and the search for new physics. In: Giulini, D., Kiefer, C., Lämmerzahl, C. (eds.) Quantum Gravity: From Theory to Experimental Search, p. 367. Springer, Berlin (2003)
Leanhardt, A.E., Pasquini, T.A., Saba, M., Schirotzek, A., Shin, Y., Kielpinski, D., Pritchard, D.E., Ketterle, W.: Cooling Bose–Einstein condensates below 500 picokelvin. Science **301**, 1513 (2003)
Loriani, S., Schubert, C., Schlippert, D., Ertmer, W., Dos Santos, F.P., Rasel, E.M., Gaaloul, N., Wolf, P.: Resolution of the co-location problem in satellite quantum tests of the universality of free fall (2020)
Lundblad, N., Carollo, R.A., Lannert, C., Gold, M.J., Jiang, X., Paseltiner, D., Sergay, N., Aveline, D.C.: Shell potentials for microgravity Bose–Einstein, condensates. npj Micrograv. **5**(1), 30 (2019)
McPherson, K., Hrovat, K., Kelly, E., Keller, J.: NASA report NP-2015-11-040-JSC: A researcher's guide to: International Space Station acceleration environment (2015)
Mossman, M., Engels, P., D'Incao, J., Jin, D., Cornell, E.: Efimov studies of an ultracold cloud of ^{39}k atoms in microgravity: Numerical modelling and experimental design. In APS Division of Atomic, Molecular and Optical Physics Meeting Abstracts, volume 2016 of APS Meeting Abstracts, pp. K1, 103 (2016)
Müntinga, H. et al.: Interferometry with Bose–Einstein condensates in microgravity. Phys. Rev. Lett. **110**, 093602 (2013)
Rudolph, J., Gaaloul, N., Singh, Y., Ahlers, H., Herr, W., Schulze, T.A., Seidel, S.T., Rode, C., Schkolnik, V., Ertmer, W., Rasel, E.M., Muentinga, H., Koenemann, T., Resch, A., Herrmann, S., Laemmerzahl, C., van Zoest, T., Dittus, H., Vogel, A., Wenzlawski, A., Sengstock, K., Meyer, N., Bongs, K., Krutzik, M., Lewoczko-Adamczyk, W., Schiemangk, M., Peters, A., Eckart, M., Kajari, E., Arnold, S., Nandi, G., Schleich, W.P., Walser, R., Steinmetz, T., Haensch, T.W., Reichel, J.: Degenerate quantum gases in microgravity. Micrograv. Sci. Technol. **23**, 287 (2011)
Sackett, C.A., Lam, T.C., Stickney, J.C., Burke, J.H.: Extreme adiabatic expansion in micro-gravity Modeling for the cold atomic laboratory. Micrograv. Sci. Technol. **30**(3), 155–163 (2018)
Williams, J., wey Chiow, S., Yu, N., Müller, H.: Quantum test of the equivalence principle and space-time aboard the international space station. J. Phys. **18**(2), 025018 (2016)